Research Article | Vol. 24, No. 26 | 26 Dec 2016 | OPTICS EXPRESS 29624

Optics EXPRESS

Surface plasmon dispersion in hexagonal, honeycomb and kagome plasmonic crystals

V. T. TENNER,* M. J. A. DE DOOD, AND M. P. VAN EXTER

Huygens-Kamerlingh Onnes Laboratorium, Leiden University, Niels Bohrweg 2, 2333 CA Leiden, The Netherlands

*tenner@physics.leidenuniv.nl

Abstract: We present a systematic experimental study on the optical properties of plasmonic crystals (PlC) with hexagonal symmetry. We compare the dispersion and avoided crossings of surface plasmon modes around the Γ-point of Au-metal hole arrays with a hexagonal, honeycomb and kagome lattice. Symmetry arguments and group theory are used to label the six modes and understand their radiative and dispersive properties. Plasmon-plasmon interaction are accurately described by a coupled mode model, that contains effective scattering amplitudes of surface plasmons on a lattice of air holes under 60°, 120°, and 180°. We determine these rates in the experiment and find that they are dominated by the hole-density and not on the complexity of the unit-cell. Our analysis shows that the observed angle-dependent scattering can be explained by a single-hole model based on electric and magnetic dipoles.

OCIS codes: (240.6680) Surface plasmons, (140.0140) Lasers and laser optics.

References and links

1. M. Fleischmann, P. J. Hendra, and A. J. McQuillan, "Raman spectra of pyridine adsorbed at a silver electrode," Chem. Phys. Lett. **26**, 163–166 (1974).
2. D. R. Smith, J. B. Pendry, and M. C. K. Wiltshire, "Metamaterials and negative refractive index", Science **305**, 788–792 (2004).
3. J. B. Pendry, D. Schurig, and D. R. Smith, "Controlling electromagnetic fields", Science **312**, 1780–1782 (2006).
4. J. K. Gansel, M. Thiel, M. S. Rill, M. Decker, K. Bade, V. Saile, G. v. Freymann, S. Linden, and M. Wegener, "Gold helix photonic metamaterial as broadband circular polarizer," Science **325**, 1513–1515 (2009).
5. N. Meinzer, W. L. Barnes, and I. R. Hooper, "Plasmonic meta-atoms and metasurfaces," Nat. Photonics **8**, 889–898 (2014).
6. J. Baumberg, M. Noginov, J. Aizpurua, K. Lin, T. Ebbesen, A. A. Kornyshev, R. Sapienza, N. van Hulst, S. Kotni, F. J. García de Abajo, P. Ginzburg, O. Hess, M. Brongersma, and S. Bozhevolnyi, "Quantum plasmonics, gain and spasers: general discussion," Farad. Discuss. **178**, 325–334 (2015).
7. F. J. Garcia-Vidal, L. Martín-Moreno, and J. B. Pendry, "Surfaces with holes in them: new plasmonic metamaterials," J. Opt. A: Pure Appl. Opt. **7**, S97 (2005).
8. N. Rotenberg, M. Spasenović, T. L. Krijger, B. L. Feber, F. J. G. de Abajo, and L. Kuipers, "Plasmon scattering from single subwavelength holes," Phys. Rev. Lett. **108**, 127402 (2012).
9. F. van Beijnum, P. J. van Veldhoven, E. J. Geluk, M. J. A. de Dood, G. W. 't Hooft, and M. P. van Exter, "Surface plasmon lasing observed in metal hole arrays," Phys. Rev. Lett. **110**, 206802 (2013).
10. V. T. Tenner, M. J. A. de Dood, and M. P. van Exter, "Measurement of the Phase and Intensity Profile of surface plasmon laser emission, ACS Photonics **3**, 942–946 (2016).
11. M. P. van Exter, V. T. Tenner, F. van Beijnum, M. J. A. de Dood, P. J. van Veldhoven, E. J. Geluk, and G. W. 't Hooft, "Surface plasmon dispersion in metal hole array lasers," Opt. Express **21**, 27422 (2013).
12. V. T. Tenner, A. N. van Delft, M. J. A. de Dood, and M. P. van Exter, "Loss and scattering of surface plasmon polaritons on optically-pumped hole arrays," J. Opt. **16**, 114019 (2014).
13. H. Saito and N. Yamamoto, "Size dependence of bandgaps in a two-dimensional plasmonic crystal with a hexagonal lattice," Opt. Express **23**, 2524 (2015).
14. W. L. Barnes, T. W. Preist, S. C. Kitson, and J. R. Sambles, "Physical origin of photonic energy gaps in the propagation of surface plasmons on gratings," Phys. Rev. B **54**, 6227–6244 (1996).
15. P. Paddon and J. F. Young, "Two-dimensional vector-coupled-mode theory for textured planar waveguides," Phys. Rev. B **61**, 2090–2101 (2000).
16. K. Sakoda, *Optical Properties of Photonic Crystals* (Springer, 2005).
17. J.-L. R. Stevens, P. Rudiger, and J. A. Bednar, "HoloViews: building complex visualizations easily for reproducible science"," in *Proceedings of the 14th Python in Science Conference,* (2015), pp. 61–69.
18. S. Adachi, *Physical Properties of III-V Semiconductor Compounds InP, InAs, GaAs, GaP, InGaAs, and InGaAsP* (Wiley, 1992).

#280449 http://dx.doi.org/10.1364/OE.24.029624
Journal © 2016 Received 8 Nov 2016; accepted 7 Dec 2016; published 13 Dec 2016

Optics EXPRESS

19. T. Okamoto and S. Kawata, "Dispersion relation and radiation properties of plasmonic crystals with triangular lattices," Opt. Express **20**, 5168 (2012).
20. M. Kerker, D.-S. Wang, and C. L. Giles, "Electromagnetic scattering by magnetic spheres," J. Opt. A: Pure Appl. Opt. **73**, 765 (1983).
21. H. Liu and P. Lalanne, "Microscopic theory of the extraordinary optical transmission," Nature **452**, 728–731 (2008).
22. F. van Beijnum, C. Rétif, C. B. Smiet, H. Liu, P. Lalanne, and M. P. van Exter, "Quasi-cylindrical wave contribution in experiments on extraordinary optical transmission," Nature **492**, 411–414 (2012).
23. H. Liu and P. Lalanne, "General properties of the surface charge pattern of one-dimensional metallic gratings," Opt. Express **21**, 16753–16762 (2013).
24. X. Zhang, H. Liu, and Y. Zhong, "Microscopic analysis of surface Bloch modes on periodically perforated metallic surfaces and their relation to extraordinary optical transmission," Phys. Rev. B **89**, 195431 (2014).
25. D. V. Coevorden, "Light propagation in ordered and disordered media," Ph.D. thesis, Universiteit van Amsterdam (1997).

1. Introduction

The interaction between surface plasmons (SPs) and nano-structures is an active field of research [1–6]. For instance, lattices of such nano-structures form optical meta-materials [5, 7]. Such materials can be designed and engineered despite the fact that the interaction with a single sub-wavelength circular nanohole in a gold film cannot be described accurately using simple theory. Near-field experiments on a single isolated hole provided more insight in such SP-hole scattering process [8], but leafs questions about the interaction between holes and the size variations that occur in arrays unaddressed. In this paper we study 10^4 holes simultaneously and retrieve more accurate information on the scattering process of individual holes than what is possible with single hole experiments.

The sub-wavelength holes are placed in a periodic crystal and a built-in light source is used to excite SPs directly. We study hexagonal, honeycomb, kagome and square lattices with similar holes. Metal-hole arrays with a square lattice and an active layer show SP-laser action [9]. The question arises how lattices with hexagonal symmetry affect such laser action. While the square lattice is two-dimensional, the observed intensity and phase of the laser beam can be described by a one-dimensional model [10]. Hexagonal lattices are intrinsically two-dimensional; their lattice vectors are not orthogonal and a two-dimensional model is necessary. A first step in this process is to determine the SP-bandstructure of such hexagonal based lattices, where the scattering properties of a single hole form a key ingredient.

In photonic crystals, the relation between bandstructure and unit cell can be described as a function of hole size and refractive index contrast. For plasmonic crystals based on nano-holes, no such relation is known, although it would greatly simplify the design process. We demonstrate that such relation also exists for metal hole arrays.

In this paper, we present accurate information about the scattering properties of individual sub-wavelength holes obtained from lattices of nano-holes. We compare plasmon scattering in square and hexagonal-based lattices, and hexagonal-based lattices with different unit cells. In the experiments, the hole size and the symmetry of the lattice and unit-cell are kept constant, while the complexity in the unit cell is increased. We show measurements of the dispersion relations around the Γ-point, present a didactic interpretation in terms of traveling waves, symmetries and group theory, and show that the observed bands are accurately described by a coupled-mode model. This model yields effective amplitudes for surface plasmons scattering on a lattice of air holes under angles of $60°$, $120°$, and $180°$. These scattering rates can be explained by a microscopic model for SP-scattering on a single hole.

2. Methods

The samples that we study consist of metal hole arrays with three different unit-cells. All 50×50 μm arrays consists of holes with diameters of 160 nm and a hole-to-hole spacing

Optics EXPRESS

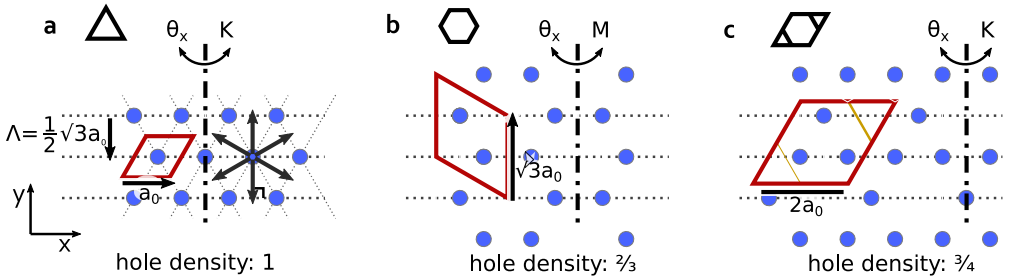

Fig. 1. Three different real space lattices and their unit cells: (a) hexagonal, (b) honeycomb, and (c) kagome. First order lattice planes are indicated with dashed lines. (a) Six traveling waves perpendicular to the lattice planes are indicated with black arrows. The rotation axis for the dispersion measurement is indicated by the dashed-dotted lines.

of $a_0 = 535$ nm. The devices are layered as follows: a 20 nm chromium film on top of a 100 nm thick Au layer, which is deposited on a dielectric substrate that comprises of a thin SiN passivation layer, an InP spacer, and 127 nm $In_xGa_{1-x}As$ (x = 0.536) gain layer on top of an InP substrate. The layer-stack is designed such that it only supports the TM-like SP-mode. Square hole arrays with a similar layer-stack are described in more detail in refs [9, 11, 12].

The SP-dispersion is measured by scanning a fiber-coupled grating-spectrometer through the back-focal-plane of a microscope objective with NA = 0.4. A thin-film polarizer in front of the fiber is used to obtain polarization sensitivity. The fiber is mounted on a motorized x-y stage and is scanned in both the Γ-M and Γ-K direction. The light is collected on the metal-air side of the sample. The SP are excited by spontaneous emission from the optically pumped InGaAs gain layer. The same setup was used in refs [9, 11, 12].

3. Theoretical background

This section presents the geometry of the studied lattices and a model to describe their SP-dispersion relations: It covers a traveling wave model, were coupling between these waves results in stop gaps, and it elucidates the connection between symmetry and radiative properties of the coupled modes.

Figure 1 shows three different lattices: hexagonal (left), honeycomb (middle) and kagome (right). These lattices share the same C_{6v} symmetry, but have different unit cells and hole densities. The typical hole spacing a_0 is kept constant, while the size a of the unit-cell changes so that the number of holes in the unit-cell increases respectively from 1 to 2 and 3. The hole density changes between the three lattices with a ratio of 1:2/3:3/4.

The dispersion relation is observed via photons that are radiated when the SP scatter on the lattice of holes. Photons emitted at a certain angle (θ_x, θ_y) have an in-plane momentum $\vec{k}_\parallel \equiv (k_x, k_y)$, with $k_x = (2\pi/\lambda_0)\sin(\theta_x)$, $k_y = (2\pi/\lambda_0)\sin(\theta_y)$. These photons are associated with SPs with 6 different momenta $\vec{k}_{sp} = \vec{G}_j + \vec{k}_\parallel$, where $\vec{G}_j$ are the lattice vectors with length $|\vec{G}_j| = 2\pi/(\sqrt{3}a_0/2)$ belonging to one of the relevant gratings [11]. These lattice vectors are indicated in Fig. 2(a). In real space, these are SP waves traveling perpendicular to the lattices planes as indicated in Fig. 1(a). The dispersion of these traveling waves is given by $\omega_j = c\,|\vec{k}_{sp}|/n_{sp}$, where n_{sp} is the effective refractive index of the SP-mode.

This uncoupled traveling wave approach already yields the main features of the dispersion relation. The dashed curves in Figs. 2(c) and 2(d) show the dispersion of uncoupled traveling waves. In the absence of SP-SP scattering, the resonance frequency at the Γ-point is given by $\omega_0 = c\left|\vec{G}_j\right|/n_{sp}$. The dashed curves have different slopes around $\theta = 0$. This slope

Optics EXPRESS

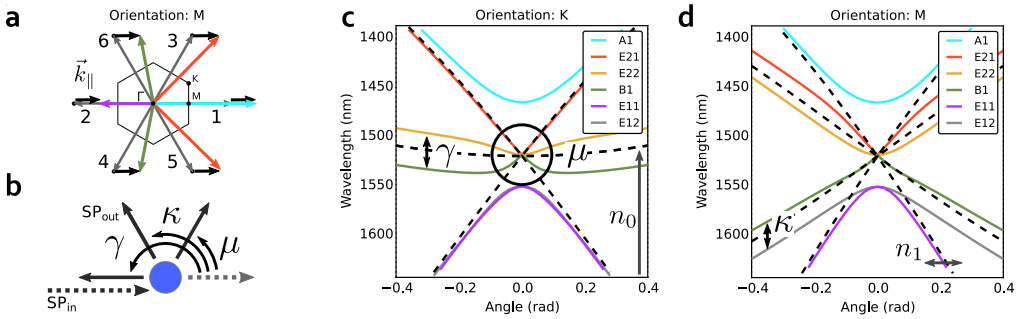

Fig. 2. Influence of SP-hole amplitude scattering on the SP-dispersion relation. (a) Reciprocal unit cell with the six resonant lattice vectors $\vec{G}_i$ (grey) and $\vec{k}_{sp}$ (colored) for $k_{\|}$(black) in the M-direction. (b) The scattering rates in three different directions. (c,d) Theoretical dispersion relation obtained from coupled mode model. The arrows indicate the influence of the scattering rates γ, κ, μ (black arrows) and energy dependent refractive index n_0, n_1 (grey arrows).

$\frac{1}{\omega}\frac{\mathrm{d}\omega}{\mathrm{d}\theta} \backsimeq \frac{1}{n_{sp,group}}\cos(\phi)$ depends on the group index $n_{sp,group}$ of the SP and the projection between the observed $\vec{k}_{\|}$ and $\vec{G}_j$. Figure 2(a) depicts $\vec{G}_j$, $\vec{k}_{\|}$ and $\vec{k}_{sp}$ for a tilt in the M direction. In the M direction, two traveling waves (k_1 and k_2) are parallel to $\vec{k}_{\|}$, which generate two non-degenerate resonances with a steep slope with $\cos(\phi) = \pm 1$. Furthermore, there are two frequency degenerate traveling waves k_3, k_5 with a slope corresponding to $\cos(\phi) = 1/2$ and two traveling waves k_4, k_6 with a slope corresponding to $\cos(\phi) = -1/2$. In total, the six traveling waves thus create four resonances. This is indicated with four dashed lines in Fig. 2(d). The dispersion relation in the Γ-K direction as depicted in Fig. 2(c) shows three double-degenerate modes as three dashed lines with slopes corresponding to $\cos(\phi) = \pm\sqrt{3}/2,\ 0$.

In order to describe the SP-dispersion relation more accurately [11, 13], we consider the surface charge $\Psi(\vec{r}, t)$, which is proportional to the out of plane $\vec{E}$-field. This surface charge $\rho(\vec{r}, t)$ is then decomposed in periodic Bloch waves:

$$\rho(\vec{r}, t) = \sum_j \rho_j(t) \exp\left(i\left(\vec{G}_j + \vec{k}_{\|}\right)\cdot\vec{r}\right), \tag{1}$$

where $\rho_j(t)$ is the time dependent amplitude and $\exp\left(i\left(\vec{G}_j + \vec{k}_{\|}\right)\cdot\vec{r}\right)$ is the spatial distribution of each plane-wave component. These plane-waves are associated with the lattice vectors $\vec{G}_j$. For the hexagonal lattices, the lowest three resonances at the Γ-point are all six-fold degenerate and a coupled-mode model with six Bloch waves suffices.

Scattering of SP on the holes causes coupling between the traveling waves, which lifts the degeneracy of the modes and creates stop gaps at the Γ-point [14, 15]. This behavior can be described by a coupled mode model for the time evolution of the Bloch waves. A similar model was used previously [11, 12] for plasmonic crystals with a square lattice. Here we extend it to hexagonal lattices. The time evolution of the surface charge can be expressed as $d\psi(t)/dt = -iH\psi(t)$, where $H(k_{\|})$ is a 6x6 matrix and $\psi(t)$ a vector with the time dependent parts $\psi_i(t)$. The eigenvalues of this matrix are the resonance frequencies at $k_{\|}$. The C_{6v} symmetry of the lattices allows us to describe the coupling with three amplitude scattering rates as depicted in Fig. 2(b): We define the 180°-scattering rate γ, the 120°-scattering rate κ, and the 60°-scattering rate μ. Analogous to ref [11], this leads to the following coupling matrix in traveling wave basis:

Optics EXPRESS

$$H = \begin{pmatrix} \omega_1 & \gamma & \mu & \kappa & \kappa & \mu \\ \gamma & \omega_2 & \kappa & \mu & \mu & \kappa \\ \mu & \kappa & \omega_3 & \gamma & \mu & \kappa \\ \kappa & \mu & \gamma & \omega_4 & \kappa & \mu \\ \kappa & \mu & \mu & \kappa & \omega_5 & \gamma \\ \mu & \kappa & \kappa & \mu & \gamma & \omega_6 \end{pmatrix} \tag{2}$$

The diagonal elements are the resonance frequencies $\omega_i = c|\vec{G}_i + \vec{k}_{\|}|/n_{sp}$ of the uncoupled traveling waves. The off diagonal elements qualify the coupling between these waves: γ for the 180° scattering within the three groups of counterpropagating waves (1,2), (3,4), (5,6), and κ and μ for the 120° and 60° scattering between waves from different groups.

Figures 2(c) and 2(d) show the influence of the three scattering rates on the dispersion relation. While their influence is mixed near the Γ-point, it is discernible at higher angles. In the Γ-K direction, the effect of the back scattering rate γ is a coupling between the degenerate traveling waves k_5 and k_6, which results in an even and odd combination with a different field distribution and a different frequency. The energy splitting induced by the 120°-scattering rate κ is visible in the Γ-M direction where it couples the degenerate waves k_3 and k_5, and k_4 and k_6. The role of 60°-scattering rate μ is mainly visible at the center of the Brillouin-zone, where all uncoupled waves are degenerate; this rate slightly alters the shape of the dispersion relation at small angles.

The highly symmetric matrix H exhibits the same C_{6v} symmetry as the lattice. We will take full advantage of this symmetry when labeling the modes and describing the number of modes and their radiative nature [16]. The symmetry determines the charge distribution of the modes (irreducible representations of the C_{6v} point group) around the holes at the Γ-point, which resembles either a monopole, dipole, quadrupole, or hexapole depending on the number of local maxima around the hole. These modes are labeled with respectively A_1, E_{1x}, E_{2x}, and B_1, as indicated in 2(c) and 2(d). Both the E_{1x} and E_{2x} modes are double degenerate. A graphical representation of these distributions can be found in ref [13].

The radiative character of the modes can be deduced from symmetry arguments. The modes at the Γ-point have different responses on the symmetry operations of C_{6v} which is expressed by their character. These different characters dictate the radiative nature of the different modes at the Γ-point. The symmetry of the mode and the symmetry of free space radiation are either the same or different. Only the dipolar E_{1x} mode is radiative perpendicular to the surface (bright), while the other three modes are non-radiative (dark).

Also the polarization of the radiated light can be deduced from symmetry arguments. For k-vectors between the Γ-point and the M- and K- point (small angles), the symmetry is reduced to C_{1h} and all modes are allowed to radiate. The modes are symmetric or antisymmetric modes under reflection in the emission plane, which is spanned by the emission direction and the surface normal. The symmetric modes couple to radiation with p-polarization (radiated $\vec{E}$ field parallel to the symmetry plane), while antisymmetric modes couple to s-polarized radiation. Compatibility relations link the modes at the Γ-point to these odd and even modes: there are three s- and three p- polarized modes in the Γ-K direction, while there are four s- and two p- polarized modes in the Γ-K direction. This difference is caused by the fact that the B_1 mode has a different character for the mirror operation over the Γ-M or Γ-K-axis.

4. Experimental results

Figure 3 shows a false color plot of the observed SP-dispersion along the Γ-K and Γ-M directions for three different lattices: hexagonal (left), honeycomb (middle), and kagome (right). The polarization of the radiation is either perpendicular (s-) or parallel (p-) to the plane spanned by $\vec{k}_{\|}$ and the surface normal. The polarization is indicated with respectively blue and yellow colors. The dashed lines in Figs. 3(a) and 3(d) show the theoretical curves from the traveling

Optics EXPRESS

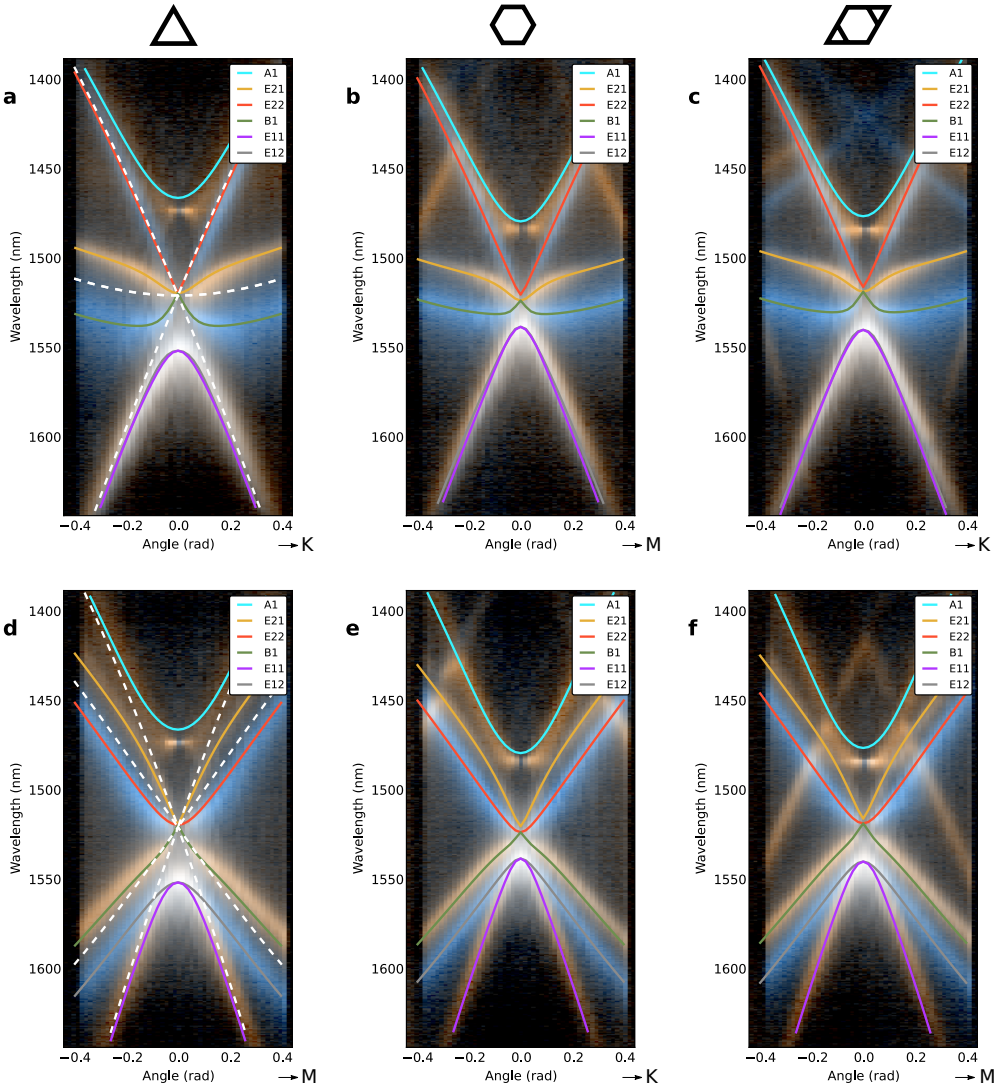

Fig. 3. Dispersion relations of (a,d) hexagonal, (b,e) honeycomb and (c,f) kagome plasmonic crystals. s- and p- polarized light is indicated with respectively blue and yellow colors. The solid lines indicate theoretical resonance frequencies.

Optics EXPRESS

wave model. The solid lines in Figs. 3(a)–3(f) show the theoretical curves from the coupled mode model. These fits yields crucial information on the SP-dynamics (see below). The dispersion shows 6 resonances, following the 6-fold symmetry. At normal incidence only 4 bands remain, of which only the degenerate bands E_{1x} radiate perpendicular to the surface ($\theta = 0$), while the other three bands are dark. There are clear frequency splittings between the A_1 and E_{2x}, B_1 and E_{1x} modes at the Γ-point. The B_1 mode almost overlaps with both E_{2x} modes. In the Γ-K direction, there are three modes (B_1, E_{11} and E_{22}) of which the out-coupled light is s-polarized and the other three modes (A_1, E_{12} and E_{21}) are a p-polarization as expected from the symmetry of the lattice. In the Γ-M direction there are two modes (E_{12} and E_{22}) radiating s-polarized light, and 4 modes (A_1, B_1, E_{11} and E_{21}) p-polarized light, as expected from the symmetry.

The honeycomb and kagome lattices exhibit some additional features: extra modes appear at higher and lower frequencies. The honeycomb and kagome lattices have larger unit cells than the hexagonal lattice, while the center of the observed dispersion relations is at the same frequency. Hence, the observed mode-crossings occur at higher order Γ-points. The honeycomb lattice is operating at the 2nd Γ-point and exhibits addition modes that intersect at higher energies, which we associate to the 3rd Γ-point. The kagome lattice is operating at the 3rd Γ-point and has extra modes on both higher and lower energies. The lower energy modes are attributed to the 2nd Γ-point. The higher order mode cannot be attributed to a Γ-point of the kagome lattice. However, inhomogeneity with a period of twice the lattice period will induce the 4th Γ-point at the wavelength of the crossing of the high energy modes. Note that at the 2nd Γ-point, relevant for the honeycomb lattice, the reciprocal space is rotated 30° compared to the 1st and 3th Γ-point and hence the M- and K-direction are interchanged.

Table 1. (a) Scattering rates for hexagonal, honeycomb and kagome lattices for scattering under 180° (γ), 120° (κ), and 60° (μ). (b) Scattering rates scaled by the relative hole-density.

a

	γ/ω_0	κ/ω_0	μ/ω_0
△	0.015 ± 0.002	0.011 ± 0.002	0.003 ± 0.002
⬡	0.009 ± 0.001	0.008 ± 0.0015	0.0035 ± 0.002
▱	0.0105 ± 0.001	0.0085 ± 0.0015	0.0025 ± 0.0015

b

$(\gamma/\omega_0)_{scaled}$	$(\kappa/\omega_0)_{scaled}$	$(\mu/\omega_0)_{scaled}$
0.015 ± 0.002	0.011 ± 0.002	0.003 ± 0.002
0.014 ± 0.001	0.012 ± 0.002	0.005 ± 0.002
0.014 ± 0.001	0.011 ± 0.002	0.003 ± 0.002

The effective amplitudes for surface plasmons scattering on a lattice of air holes are retrieved by comparing the experimental data with our model. As discussed before, different parts of the dispersion relation contain information on different scattering rates. These features are easily identified by eye; the model's resonance wavelengths are overlayed graphically [17] with the measurements and the scattering rates are adjusted by hand. The errors are estimated by adjusting a parameter until the overlap was clearly reduced. Hence the reported errors are interpreted as 2σ deviations. This procedure was performed independently by each of us and the resulting parameters were in accordance with each other within the errors estimated by each researcher. These values are presented in Table 1a (discussion follows below).

In order to retrieve a good fit of the modes at high and low energies, the dispersion of the refractive index should be taken into account. The effective refractive index shows dispersion due to the electronic structure of the media. This is included as a perturbation n_1 on the refractive index: $n_{sp}(\lambda) = n_0 + n_1 \lambda/\lambda_0$, which mainly influences the shape of the modes at high and low energies. The fitted refractive index n_0 is 3.28 ± 0.005 and n_1 is 0.35 ± 0.15 for all lattices, a straightforward calculation shows that this dispersion n_1 is created by both the gain layer [18]

Optics EXPRESS

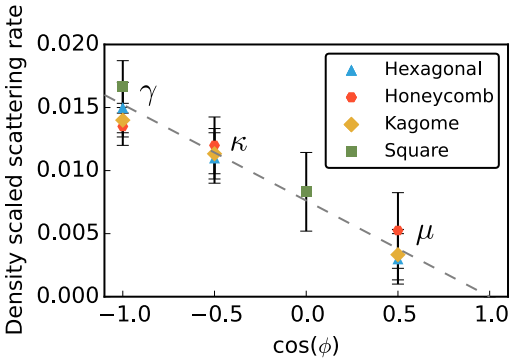

Fig. 4. Scattering rates scaled to the hole-density of the hexagonal lattice as function of scattering angle ϕ for scattering under 180° (γ), 120° (κ), and 60° (μ). The scattering rates for 180° and 90° are taken from ref [12]. The dashed line indicates $a - b\cos(\phi)$ for $a/b = 1$.

and gold layer.

The fitted scattering rates of the three different lattices parameters are shown in Table 1a. The backscatter rate γ is clearly larger than the 120°-scattering rate κ which is again larger than the 60°-scattering rate μ. The main uncertainty in the determination of the 60°-scattering rate μ arises from the dark nature of the A_1, B_1, and E_{2x} modes, limiting the visibility at the location of the dispersion relation that is most sensitive to μ. The scattering rates of the triangular lattice are larger than these of the kagome lattice which are larger than these of the honeycomb lattice. We attribute these differences to changes in the hole density in these three lattices (see below).

5. Discussion

All three scattering rates originate from the same physical effect: SP-scattering on subwavelength holes, and hence they are expected to depend on both the hole-density and the scattering cross-section of the holes. Table 1b shows the scattering rates scaled to the hole density of the hexagonal lattice, which corresponds to a multiplication by a factor $3/2$ for the honeycomb and $4/3$ for the kagome lattice. The good overlap between the scaled scattering rates demonstrates the proposed hole-density dependence. Hence, the scattering rates are mainly set by the hole-density, and less by the complexity of the unit-cell.

Figure 4 shows the scattering rates dependence on the scattering angle ϕ. The angle dependence of the scattering rates can be described by the equation $a - b\cos(\phi)$, indicated in Fig. 4 with the dashed line as guide to the eye. This line predicts that the forward scattering is zero. A physical interpretation follows below.

We first compare our results with earlier work on SP scattering in square [11] and hexagonal lattices [13, 19]. The reported scattering rates for square lattices [11] with a similar layer stack and hole size are $\gamma/\omega_0 = 0.016 \pm 0.02$ for 180°-scattering and 0.008 ± 0.003 for 90°-scattering. After scaling these results with the relative hole density ($\rho/\rho_0 = 1.03$), they are added to Fig. 4; the 180°-scattering overlaps very well with our results for hexagonal-based lattices, and also the extra datapoint at 90°-scattering neatly follows the $\cos(\phi)$-relation.

For completeness, we will also compare our results with the scarce previous efforts [13, 19]. Scattering rates of hexagonal plasmonic crystals were not reported yet, but these can be extracted from the dispersion relations in refs. [13, 19] using the procedure explained above. We take the results for hole sizes ($d/a = 0.34$) that are comparable to our sample. From the simulations in ref [19], we extract scattering rates $\gamma/\omega_0 = 0.0040 \pm 0.0010$, $\kappa/\omega_0 = 0.0028 \pm 0.0003$ and $\mu/\omega_0 = 0.0004 \pm 0.0003$. In the measurements of ref [13] the A-band of sample with the

Optics EXPRESS

relevant hole sizes is outside the observed wavelength range. Instead, we extrapolate this band with a spline and extract scattering rates $\gamma/\omega_0 = 0.050 \pm 0.010$, $\kappa/\omega_0 = 0.010 \pm 0.010$, and $\mu/\omega_0 = 0.002 \pm 0.010$. Even though these scattering rates were observed at shorter wavelengths in the visible ($\lambda \sim 600$ nm), they are comparable in magnitude to our results. Furthermore, also the sequence of the scattering rates is the same: backscatter rate γ is larger than the $120°$-scattering rate κ, which in turn is larger than the $60°$-scattering rate μ.

The proposed $a - b\cos(\phi)$ dependence of the scattering rate is based on the SP-scattering of a single small cylindrical hole. This scattering process can be described by an effective electric $\vec{p}$ and magnetic $\vec{m}$ dipole [8]. In this model the incident SP-wave excites with these dipoles, which then radiate partially to SP-waves again. SP-waves are mainly TM polarized, and hence the out-of-plane component p_z of the electric dipole and the in-plane component m_y of the magnetic dipole dominate the scattering process. Both dipoles have a distinct in-plane scattering profile; the electric dipole p_z radiates isotropically, while the magnetic dipole m_y radiates dominantly in the forward and backwards directions. The scattered field consists of a combination of these dipole responses, and yield a combined scattering amplitude $a - b\cos(\phi)$ with

$$\frac{b}{a} = \sqrt{\frac{\epsilon+1}{\epsilon}}\frac{m_y}{p_z} = \left(\frac{\epsilon+1}{\epsilon}\right)\frac{-\alpha_m}{\alpha_p}, \tag{3}$$

where α is the polarizability of a single hole. The factor $\sqrt{\frac{\epsilon+1}{\epsilon}}$ accounts for the small difference in the ratio H/E for confined SPs compared to free space electro-magnetic waves [8]. The ratio between the permitivities $\epsilon = \epsilon_{metal}/\epsilon_{dielectric} = -10$ for our system, and hence this factor is close to 1. Figure 1(b) shows the scattering rates as function of $\cos(\phi)$. The scattering rates overlap with a line that crosses the $\cos(\phi)$-axis at $\cos(\phi) = 1$, which indicates that the forward scattering is zero, suggesting that $|\vec{p}| \simeq |\vec{m}|$. This corresponds to the second Kerker condition [20], in which a hole acts as a Huygens-reflector. The supplemental information of ref. [8] calculates the polarizabilites α_m and α_p for holes in perfectly conducting metal film on a glass substrate, where a surface plasmons are traveling on the metal-air interface. For our relative hole radius $d/\lambda = 0.18$ this theory predicts that the polarizabilities have an opposite sign and a ratio $-\alpha_m/\alpha_p \approx 3.5$. For a smaller hole radius this ratio increases to 1.7 for zero radius. However, our experimental data indicate that the ratio is $\simeq 1$ for our geometry. This quantitative discrepancy might result from the following: Our SP scattering process is more complicated than captured in the calculations of the dipole model, because our SPs are scattering on holes filled with air, while they are traveling on the metal-semiconductor interface and the metal-air interface contains a chromium layer to damp the SP. The current calculations on the dipole model, assume the same index for both medium and hole as well as a perfectly conducting metal, where no field penetrates in. For a realistic gold film the optical penetration-depth at telecom-frequencies is typically ≈ 20 nm, resulting in a slightly higher effective hole diameter.

We find a qualitative agreement between the dipole model and our measurements. This is surprising, because there are two reasons why a description based on single-hole SP-scattering might be too simple. First of all, this dipole model does not take quasi cylindrical (or creeping) waves into account, while they carry more than 40% of the field at short (< 2.5 μm) distances [8] and they are typically responsible for half of the extra-ordinary transmission through metal hole arrays [21, 22]. However, there is no influence of quasi-cylindrical waves visible in our measurements, because the dispersion relation is formed by interference between scattered waves from many holes. The propagation distance of SP is much larger than for quasi-cylindrical waves and hence SPs dominate the dispersion [23, 24]. Finally, the dipole model describes the response of a single hole, while we observe the response of a lattice of holes. Hence, one might expect that lattice effects and multi-hole phenomena, such as coherent addition of the scattering of all holes and hole-hole (dipole-dipole) interaction, will become important. The current experiments

Optics EXPRESS

do not yet have sufficient control to distinguish these effects, and detailed theory is absent: even for a lattice of only electric dipoles this is already a non-trivial exercise [25], where the magnetic dipoles are ignored due to their complexity. Hence, this remains a future challenge.

6. Conclusions

We experimentally studied the scattering properties of three different metal-hole-array plasmonic crystals with hexagonal lattices, but different unit-cells. The unit cells have the same symmetry, but an increasing number of holes and complexity. We compare the observed dispersion relations with a coupled mode model, which yields the amplitude scattering rate of surface plasmons on a lattice of metal holes under three different angles: $60°$, $120°$, and $180°$. We find that the influence of the three different lattices on the scattering rates is dominated by the hole-density. The symmetry of the lattice only selects the allowed scattering angles by constructive interference, but does not influence the individual scattering rates. Furthermore, we find that the angle dependence of the scattering rates shows a qualitative, but no quantitative, agreement with a single-hole dipole approximation that takes only the SP-mode into account. Hence, we conclude that lattice effects and hole-hole (dipole-dipole) interaction are less important than the single hole response.

Acknowledgments

The authors thank Philippe Lalanne and Haitio Liu for the discussions about quasi-cylindrical waves, and Peter J van Veldhoven and Erik Jan Geluk for their help in fabricating the samples at the COBRA Research Institute of the Technische Universiteit Eindhoven, The Netherlands. This work is part of the research program of the Foundation for Fundamental Research on Matter (FOM), which is part of the Netherlands Organization for Scientific Research (NWO).